Since January 2020 Elsevier has created a COVID-19 resource centre with free information in English and Mandarin on the novel coronavirus COVID-19. The COVID-19 resource centre is hosted on Elsevier Connect, the company's public news and information website.

Journal of Molecular Structure 1265 (2022) 133480

Contents lists available at ScienceDirect

Journal of Molecular Structure

journal homepage: www.elsevier.com/locate/molstr

Metal complexes of thiosemicarbazones derived by 2-quinolones with Cu(I), Cu(II) and Ni(II); Identification by NMR, IR, ESI mass spectra and *in silico* approach as potential tools against SARS-CoV-2

Ashraf A Aly[a,*], Elham M. Abdallah[a], Salwa A. Ahmed[a], Mai M. Rabee[a], El-Shimaa M.N. Abdelhafez[b]

[a] *Chemistry Department, Faculty of Science, Minia University, El-Minia 61519, Egypt*
[b] *Medicinal Chemistry, Department, Faculty of Pharmacy, Minia University, El-Minia 61519 Egypt*

ARTICLE INFO

Article history:
Received 8 October 2021
Revised 17 May 2022
Accepted 7 June 2022
Available online 9 June 2022

Keywords:
2-Quinolones
Thiosemicarbazones
Cu(I)
Ni (II) and Cu(II) salts
Monodentate
Bidentate
ESI
NMR
Molecular docking
Anti-Covid agents

ABSTRACT

Substituted thiosemicarbazones derived by 2-quinolone were synthesized to investigate their complexation capability towards Cu(I), Cu(II) and Ni(II) salts. The structure of the complexes was established by ESI, IR and NMR spectra in addition to elemental analyses. Monodetate Cu(I) quinoloyl-substituted ligands were observed, whereas Ni(II) and Cu(II) formed bidentate-thiosemicarbazone derived by 2-quinolones. Subsequently, molecular docking was used to evaluate each analog's binding affinity as well as the inhibition constant (*ki*) to RdRp complex of SARS-CoV-2. Docking results supported the ability of the tested complexes that potentially inhibit the RdRp of SARSCov-2 show binding energy higher than their corresponding ligands. Additionally, ADMET prediction revealed that some compounds stratify to Lipinski's rule, indicating a good oral absorption, high bioavailability good permeability, and transport *via* biological membranes. Therefore, these metals-based complexes are suggested to be potentially good candidates as *anti*-covid agents.

1. Introduction

Thiosemicarbazones (TSCs) have attracted considerable attention by chemists and biologists because of their wide range of pharmacological effects such as antibacterial [1], antiviral [2], antifungal [3] and particularly [4], antitumor [5] and antileukemic [6] activities. Previously, it was shown that 4-acetylaminobenzaldehyde thiosemicarbazone was used to treat tuberculosis [7]. In the same manner, 2-formyl-pyridine thiosemicarbazone showed potent anticancer activity [8]. Previously, 3-aminopyridine-2-carboxaldehyde thiosemicarbazone (Triapine) is an extensively studied as TSC for cancer chemotherapy [9–15].

Thiosemicarbazones (TSCs) have shown the formation of metal complexes towards various transition metals including Cu, Pd, and Ni. The impact of TSCs on topoisomerase αII (Top2) has been noted several times, and the exact mechanism was initially unclear, though it appeared to involve increases in DNA cleavage [16]. The ability to impact Top2 function was also used to design Cu-radiolabeled TSC complexes in order to track topoisomerase Top2 expression in tumor tissue [17,18]. Analysis of the metal ion such as Cu(II) was found as essential for TSC activity Top2 [19]. Recent reported approach of some thiosemicarbazones were evaluated for their dipeptidyl peptidase-4 (DPP-4) inhibitory effects based upon a convenient fluorescence-based assay [20]. One of these derivatives was identified as the most effective DPP-4 inhibitor in this series with an IC_{50} value of 1.266 ± 0.264 nM, when compared with sitagliptin as a reference (IC_{50} = 4.380 ± 0.319 nM) [20]. Molecular docking studies indicated that compound presented π-π interactions with Arg358 and Tyr666 [20].

Recently, 4-(1-adamantyl)-3-thiosemicarbazones have been evaluated for their *in vitro* activities against some Gram-positive, Gram-negative bacteria, fungus Candida albicans and cytotoxicity against four cancer cell lines (Hep3B, HeLa, A549, and MCF-7) [21].

Complexation of several thiosemicarbazones employing Cu(II) acetate hydrate, analytical and spectroscopic data for the isolated complexes, revealed that in most cases a reduction to copper(I) occurrence [22]. Although, other literatures showed the stability of thiosemicarbzaones of either Cu(I)- and/or Cu(II) complexes [23,24]. Cu(I) is a soft metal ion and hence prefers soft donor

* Corresponding author.
E-mail address: ashrafaly63@yahoo.com (A.A. Aly).

https://doi.org/10.1016/j.molstruc.2022.133480
0022-2860/

sites like sulfur [25]. It is also well known that thiosemicarbazones coordinate as bidentate ligand through azomethine nitrogen and thione/thiolate sulfur [25].

The COVID-19 pandemic poses an unprecedented challenge for the rapid discovery of drugs against this life-threatening disease. Owing to the peculiar features of the metal centers that are currently used in medicinal chemistry, metallodrugs might offer an excellent opportunity to achieve this goal. Copper in different formats has been used in research and clinical settings to reduce the risk of bacterial and viral contamination [26]. In the last three decades, several efforts have been made to develop suitable antiviral by using thiosemicarbazide scaffold. Its hybridization with other pharmacophores has been used as a strategy to enhance safety and efficacy [27]. Recently, it has reported that complexes of cobalt(III) with 2-acetylpyridine-*N*(4)-*R*-thiosemicarbazones showed activity against *Mycobacterium tuberculosis*, whereas their minimal inhibitory and minimal bactericidal concentrations (MIC and MBC) were determined. Some of these complexes of cobalt- thiosemicarbazones also showed *in vitro* and cell viability as antiviral potential reagents against chikungunya virus infection (CHIKV). They revealed promising MIC and MBC values which ranged from 0.39 to 0.78 μg/mL found in two tested strains and presented high potential against CHIKV by reducing viral replication up to 80%. In addition, the molecular docking analysis was performed whereas, the relative binding energy of the docked compound with five bacteria strains was found in the range of E = 3.45 and E = 9.55 kcal/mol [28].

In the global pandemic caused by SARS-CoV-2, there is an emergence of the need for a treatment modality. Repurposing of the antimalarial/antiviral drugs such as chloroquine, Galidesivir, Remdesivir, Tenofovir, Sofosbuvir, Ribavirin, etc. was recommended for the treatment of COVID-19. These drugs would inhibit the RdRp complex of SARS-CoV-2 whereas, the molecular docking studies revealed the binding energy between RdRp and the drugs to be -5.1, -7.0, -7.6, -6.9, -7.5, -7.8 kcal mol^{-1}, respectively [29]. Comparison of the available drugs, the antiviral metal complexes have been reported to exhibit great potential acting as a better alternative of these drugs with binding energies in the range of -4.4 to -10.24 kcal mol^{-1} [29]

Current molecular docking studies revealed that complex of ferroquine derivative of Fe(II), Ni (II) and Pt-based thiosemicarbazone complexes showed better binding affinity of -10.24, -8.95, -8.09, and -8.6 kcal mol^{-1}, respectively. These complexes displayed RdRp of SARS-CoV-2 to probably work better than the current drugs to prevent SARS-CoV-2. Therefore, they displayed further *in vitro/in vivo* application of the metal-based compounds against SARS-CoV-2.

Suitable design of the ligands could result in robust transition metal complexes that are thermodynamically, kinetically and redox stable and suitable for *in vivo* applications against a wide range of diseases [30]

Utilizing by our previous synthesis of thiosemicarbazones **1a-f** [31], metal complexes of their Cu(I), Ni (II) and Cu (II) were designed, synthesized and tested computationally as *anti*-SARS-CoV-2 candidates using molecular docking calculations as well as *in silico* ADMET prediction software.

2. Experimental section

Melting points were recorded using a Gallenkamp melting point apparatus (Gallenkamp, UK) and open capillaries. Melting points are uncorrected. ^{1}H and ^{13}C NMR spectra were measured utilizing by Bruker Avance (400 MHz for ^{1}H, and 100 MHz for ^{13}C) at Institute of Technology, Karlsruhe University, Karlsruhe, Germany. The ^{1}H and ^{13}C chemical shifts were recorded relative to internal standard TMS. Mass spectrometry was performed using electron impact at 70 eV, (FAB-MS): Finnigan MAT 95 at Institute of Organic Chemistry, Karlsruhe Institute of Technology, Karlsruhe, Germany. Elemental analyses were carried out at Karlsruhe Institute of Technology, Karlsruhe, Germany. Mass spectra were recorded on a Varian MAT 312 instrument in EI mode (70 eV), at Institute of Organic Chemistry, Karlsruhe Institute of Technology, Karlsruhe, Germany. IR spectra were performed using KBr pellets that were run on a FT-IR (Bruker) at Institute of Organic Chemistry, Karlsruhe Institute of Technology, Karlsruhe, Germany. Preparative thin layer chromatography (plc) and glass plates (20 × 48 cm) were covered with a slurry of silica gel (Merck PF_{254}) then air dried and developed using the solvents listed. Zones were detected by quenching of the indicator fluorescence upon exposure to 254 nm UV light.

Table 1
Some physical data and yield in g (%) of complexes **5a-c** and **7a-h**.

No	Complex	Color	m.p. (°C)	Yield g (%)
1	**5a**	Pale red	>350	0.0278 g (57%)
2	**5b**	Pale red	>350	0.0289 g (60%)
3	**5c**	Pale red	>300	0.0218 g (45%)
4	**7a**	Dark green	> 330	0.0073 g (52%)
5	**7b**	brown	>330 (decomp.)	0.0160 g (75%)
6	**7c**	Dark brown	>340 (decomp.)	0.0029 g (78%)
7	**7d**	brown	>348 (decomp.)	0.0069 g (76%)
8	**7e**	Buff	>350	0.0180 g (24%)
9	**7f**	Yellow	>350	0.0327 g (39%)
10	**7g**	Buff	>350	0.0427 g (55%)
11	**7h**	Buff	>350	0.0536 g (62%)

2.1. Preparation of ligands; hydrazinecarbothioamide derivatives 3a-f

A mixture of thiosemicarbazide (**2**) (0.83 g, 9.1 mmol) and the appropriate aldehydes **1a-f** (9.1 mmol) in 100 mL of a mixture of ethanol 50 mL together with equivalent amount of glacial acid (1:1) was heated under reflux with stirring for 6–8 h. The yellow precipitate was allowed to stand, filtered off, washed with ethanol, dried and recrystallized from the stated solvents. The data of the formed products were confirmed as those reported in literature [31].

Preparation of organometallic thisemicarbazone/quinoline-2-ones

2.2. General procedure for synthesis of Cu(I)-thiosemicarbazones 5a-c

A mixture of 0.1 mmol of **3a,b** and 0.1 mmol of Cu(I) salts **4a,b** in 20 mL CH_3CN was stirred at room temperature for 24 h. The formed precipitate was then washed with H_2O (100 mL) and followed by washing with 100 mL EtOH. The obtained complexes **5a-c** were well-dried. Physical and analytical data of 2-quinolyl-thiosemicarbazones and their Cu(I) were illustrated in Tables 1 and 2.

2.3. General procedure for synthesis of Ni(II) and Cu(II)-thiosemicarbazones 7a-h

A mixture of 0.01 mmol of **3a-f** and 0.01 mmol of Ni (II) or Cu(II) salts **6a-c** in 50 mL CH_3OH was refluxed for 6-10 h. The formed precipitate was then rinsed with H_2O (100 mL) followed by washing with 100 mL EtOH. The obtained complexes were well-dried. The physical and analytical data of the obtained products **7a-h** were illustrated in Tables 1 and 2.

2.4. Molecular docking study

Docking simulation study was carried out using Molecular Operating Environment (MOE®) version 2014.09, Chemical Comput-

Table 2
Physical and analytical data of 2-quinolyl-thiosemicarbazones complexes of Cu(I) **5a-c**, Ni(II) **7a-d** and Cu(II) **7e-h**.

No	Ligand	Metal salt	Complex	Stoichiometry	Molecular formula	C H N S
1	**3a**	CuI	**5a**	1:1	$C_{11}H_9ClIN_4O_2SCu$	Calcd: C, 27.12; H, 1.86; N, 11.50; S, 6.58 Found: C, 27.30; H, 2.00; N, 11.40; S, 6.70
2	**3b**	CuBr	**5b**	1: 1	$C_{11}H_9Br_2N_4O_2SCu$	Calcd: C, 27.26; H, 1.87; N, 11.56; S, 6.62 Found: C, 27.50; H, 2.20; N, 11.60; S, 7.40
3	**3b**	CuI	**5c**	1:1	$C_{11}H_9BrN_4O_2SCu$	Calcd: C, 24.85; H, 1.71; N, 10.54; S, 6.03 Found: C, 24.70; H, 1.58; N, 10.30; S, 6.00
4	**3a**	$NiCl_2$	**7a**	2:1	$C_{26}H_{28}ClN_8O_4S_2\ Ni_2$	Calcd: C, 42.57; H, 3.85; N, 15.28; S, 8.74 Found: C, 42.40; H, 4.00; N, 15.30; S, 8.90
5	**3b**	$NiCl_2$	**7b**	2:1	$C_{22}H_{18}Br_2ClN_8O_4S_2Ni_2$	Calcd: C, 31.64; H, 2.17; N, 13.42; S, 7.68 Found: C, 31.50; H, 2.00; N, 13.30; S, 7.55
6	**3c**	$NiCl_2$	**7c**	2:1	$C_{22}H_{20}ClN_8O_4S_2Ni_2$	Calcd: C, 39.01; H, 2.98; N, 16.54; S, 9.47 Found: C, 39.20;.H, 3.10; N, 16.40; S, 9.60
7	**3d**	$NiCl_2$	**7d**	2:1	$C_{24}H_{24}ClN_8O_4S_2Ni_2$	Calcd: C, 40.95; H, 3.50; N, 16.00; S, 9.12 Found: C, 40.86; H, 3.43; N, 15.88; S, 9.09
8	**3a**	$CuCl_2$	**7e**	2:1	$C_{22}H_{18}Cl_3N_8O_4S_2Cu_2$	Calcd: C, 34.95; H, 2.40; N, 14.82; S, 8.48 Found: C, 34.80; H, 2.50; N, 15.00; S, 8.28
9	**3b**	$CuCl_2$	**7f**	2:1	$C_{22}H_{18}Br_2ClN_8O_4S_2Cu_2$	Calcd: C, 31.27; H, 2.15; N, 13.26; S, 7.59 Found: C, 31.40; H, 2.30; N, 13.30; S, 7.70
10	**3a**	$Cu(CH_3COO_2)_2$	**7g**	2:1	$C_{24}H_{21}Cl_2N_8O_6S_2Cu_2$	Calcd: C, 36.97; H, 2.72; N, 14.37; S, 8.23 Found: C, 37.10; H, 2.60; N, 14.50; S, 8.40
11	**3b**	$Cu(CH_3COO_2)_2$	**7h**	2:1	$C_{24}H_{21}Br_2N_8O_6S_2Cu_2$	Calcd: C, 33.19; H, 2.44; N, 12.90; S, 7.38 Found: C, 33.30; H, 2.60; N, 13.10; S, 7.50

Scheme 1. Synthesis of 2-quinlonylthiosemicarbazones **3a-f**.

ing Group Inc., Montreal, Canada. The computational software operated under "Windows XP" installed on an Intel Pentium IV PC with a 1.6 GHz processor and 512 MB memory. The target compounds were constructed into a 3D model using the builder interface of the MOE program and docked into the active site of RdRp complex of SARS-CoV-2. (PDB ID: 6M71). After that checking their structures and the formal charges on atoms by 3D depiction, were carried out.

3. Results and discussion

Scheme 1 outlines the preparation of ligands 3a-f as previously shown in literature [31]. Thus, upon mixing equimolar amounts of **3a,b** and Cu(I) salts **4a,b** in CH_3CN and the mixture was stirred for 24 h, metal complexes **5a-c** were obtained (Scheme 2). Similarly, on refluxing **3a-f** with Ni(II) and Cu (II) salts **6a-c** in CH_3OH, the bidentate metal complexes **7a–h** (Scheme 3) were obtained. Some physical data and yield in g (%) of complexes **5a-c** and **7a-h**. are shown in Table 1.

3.1. Assignment of the complexes 5a-c and 7a-h by elemental analyses and mass spectra

Elemental analyses of the obtained metal complexes **5a-c** and **7a-h** are as shown in Table 2. ESI-MS is used to analyze metal species in a variety of samples. Here, we describe an application for identifying metal species by tandem mass spectrometry (ESI-MS/MS) with the release of free metals from the corresponding metal–ligand complexes. This method can be used for identifying different metal–ligand complexes, especially for metal species whose mass spectra peaks are clustered close together. The complexation of these donor groups suffered significant negative shifts confirming the effective coordination of these groups with the metal center showed the positive exact masses and isotope distribution patterns of the ESI of complexes of compounds and the corresponding formed simulated metal complex between **3a** with CuI (**4a**) and **3b** with **4a** (Figs 1 and 2). For example, positive exact masses and isotope pattern, both experimentally and simulated of the formed metal complex **5a** formed between **3a** and **4a**, as an example (Fig. 1). The simulated molecular formula of $C_{11}H_8ClN_4O_2SCu$ appeared exactly with the experimental ESI of the complex. In case of **5b**, the molecular peak was found as the base peak and appeared at m/z = 403.88 (Fig. 2). In case of the mass spectrum of metal complex **7c** (Fig. 3), the molecular ion peak supported the chemical formula as $C_{22}H_{20}N_8O_4S_2Ni_2$ with an exact mass: 639.98.

3.2. Assignment by IR spectra

The assignments of the IR bands are useful for determining the ligand's mode of coordination are listed in Table 3. The bands for compounds **5a-c** and **7a-h** were absorbed in the region at

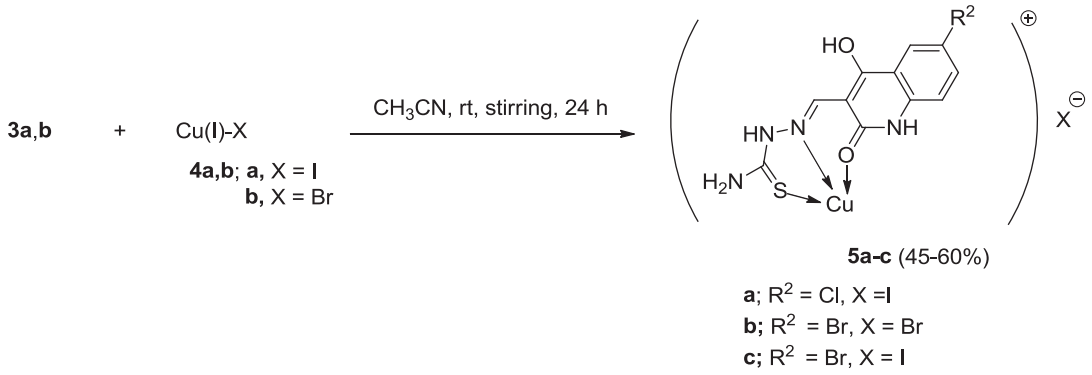

Scheme 2. Synthesis of 2-quinlonylthiosemicarbazones-Cu(I) complexes **5a-d**.

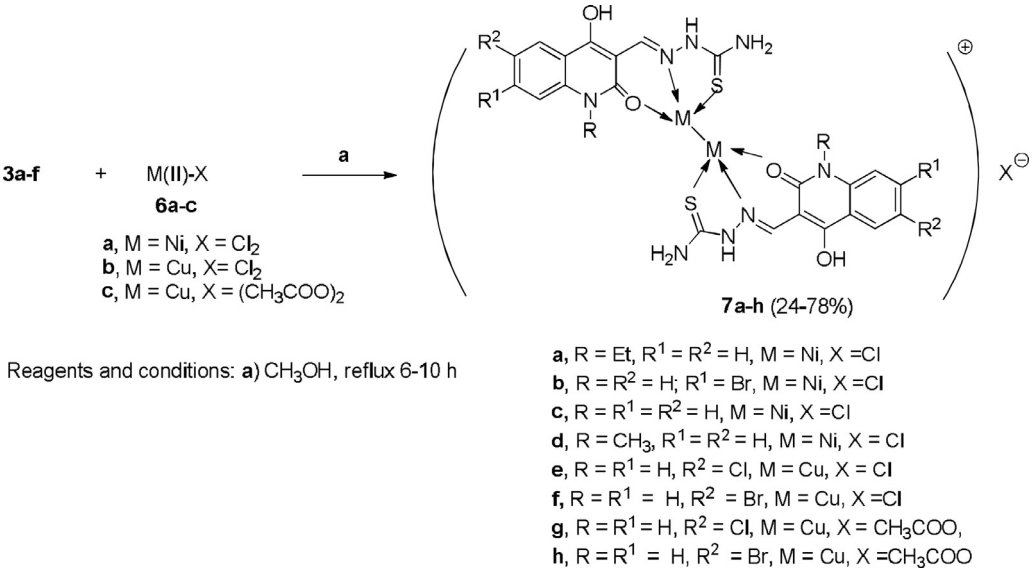

Scheme 3. Synthesis of 2-quinlonylthiosemicarbazones-Ni (II) and Cu (II) complexes **7a-h**.

ν = 3450–3400 cm^{-1} for the OH stretching vibration. Two stretching vibration bands at ν = 3356–3260 and 3150-3235 cm^{-1}, attributed to the symmetrical NH_2 and NH, respectively. The shift in functional groups from the ligands to the corresponding complexes supported the chelating process. Coordination occurred *via* the sulfur of thione, together with the oxygen of the carbonyl and the nitrogen of azomethine. The center of coordination was supported by the appearance of a strong bending vibration band for **3a** as an example, at ν = 850 cm^{-1} in the spectrum of thiosemicarbazone is mainly due to the C=S bending frequency. This band is found to be shifted to ν = 860 cm^{-1} in the spectra of complex **5a** (Table 3, Fig. 4). The increasing of the wave number upon complexation indicates a considerable change in bond order and the formation of a metal-sulfur bond [27]. This was obviously observed with the variation of functional groups corresponding to nitrogen of azomethine, oxygen of the carbonyl and sulfur of thione group (Table 3) along with the appearance of bending vibration band corresponding to M-N group e.g. for **5a** at λ_{max} = 560 nm.

The same trend was also noted for ligands **3a-f** as well as their corresponding metal complexes **7a-h** (Table 3). For example, the band of quinolonyl-CO bands of complex 3a appeared at stretching vibration frequencyν = 1665 cm^{-1}, which was shifted to ν = 1678 cm^{-1} (Fig. 5) indicating coordination of the carbonyl oxygen. Also, the wavenumber of thione sulfur in **3a** appeared at bending vibration frequency ν = 850 cm^{-1} which was shifted in case of **7a** to ν = 870 cm^{-1}, indicating the coordination of the sulfur lone pair of the thione group with the metal. Moreover, the nitrogen of the azomethine in **3a** was shown at stretching vibration frequency ν = 1608 cm^{-1} that was shifted to ν = 1620 cm^{-1} upon complexation into **7a** (Fig. 5). In general, the IR spectra indicated the coordination of the nitrogen of azomethine group, the sulfur of thione and oxygen of the quinolonyl-carbonyl group.

3.3. Assignment by NMR spectra

Utilized by elemental analyses, mass-, IR- and the chemical shifted in NMR-spectra, the structure of the complexation process was confirmed (Table 4). As examples, Fig. 6 showed the remarkable shifts in chemical shifts (δ) in ^{1}H NMR of compounds **3a,b** and their complexes **5a-c**. NMR spectroscopic data were distinguished for compounds **5a-c** for Cu(I) complexes due to the paramagnetic property of Cu(I). However, Ni(II) and Cu(II) complexes didn't show any distinguished bands due to the diamagnetic properties of Ni(II) and Cu(II) Fig 7.

One can conclude that the formed metal complexes could be either in its cationic-anionic form or in is acidic form, which exceeded by a proton from the proposed structure. As for example, the molecular formula of compound **5a'** is exceeded by a hydrogen proton (Fig. 8). The exact molecular formula of **5a**, as an ex-

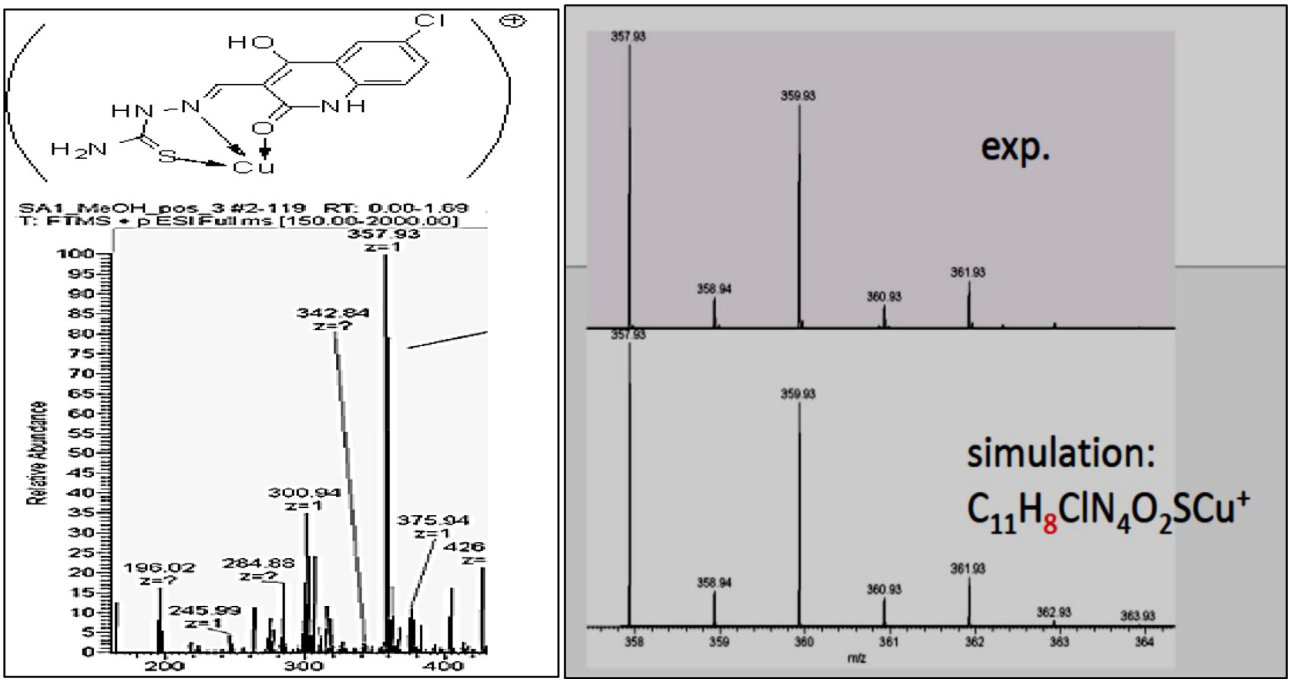

Fig. 1. Positive exact masses and isotope pattern, both experimentally and simulated mass spectra of the metal complex **5a** formed between **3a** and Cu(I)I.

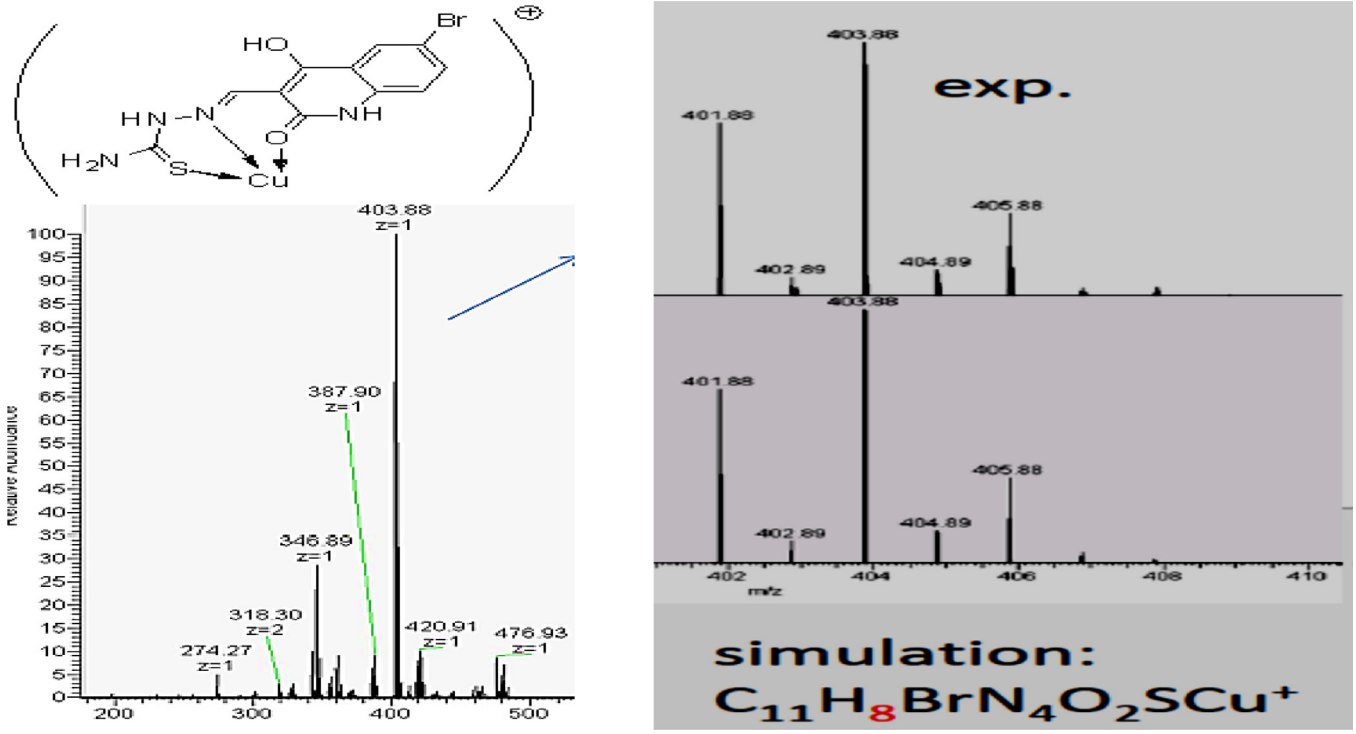

Fig. 2. Positive exact masses and isotope pattern, both experimentally and simulated mass spectra of the formed metal complex **5b** formed between **3b** and Cu(I)I.

ample, was in a good agreement with the molecular formula of $C_{11}H_8ClCuN_4O_2S$ (Fig. 8).

3.4. Computational analysis

3.4.1. Docking studies

Molecular modeling study was performed through docking most of the target organometallic complexes **5a,b** and **7a-f** at the RdRp complex of SARS-CoV-2 using Molecular Operating Environment (MOE®) version 2014.09. Complexes of the same metal and different anion were not studied. The crystal structure of RdRp was obtained from the PDB with PDB ID: 6M71 [32]. Molecular docking is *in silico* computer algorithm used to estimate two main terms; the first is to evaluate the appropriate pose (orientation & conformation) of the target compounds inside the binding site in comparison to that of their starting ligands **3a-f** and the second is the computation of the docking scoring (C-docker energy), in order to provide us with information about the interactions between the

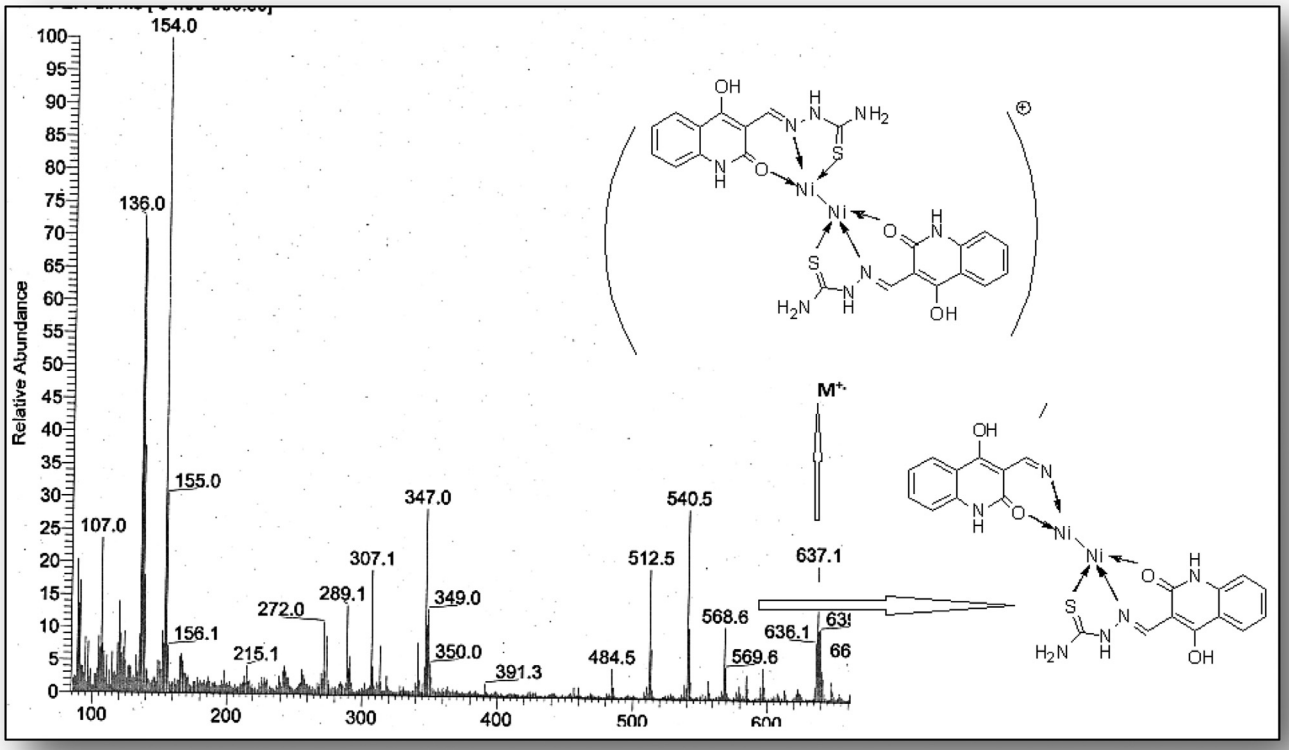

Fig. 3. FAB mass spectrum of the formed metal complex **7c** from **3c** and $NiCl_2$.

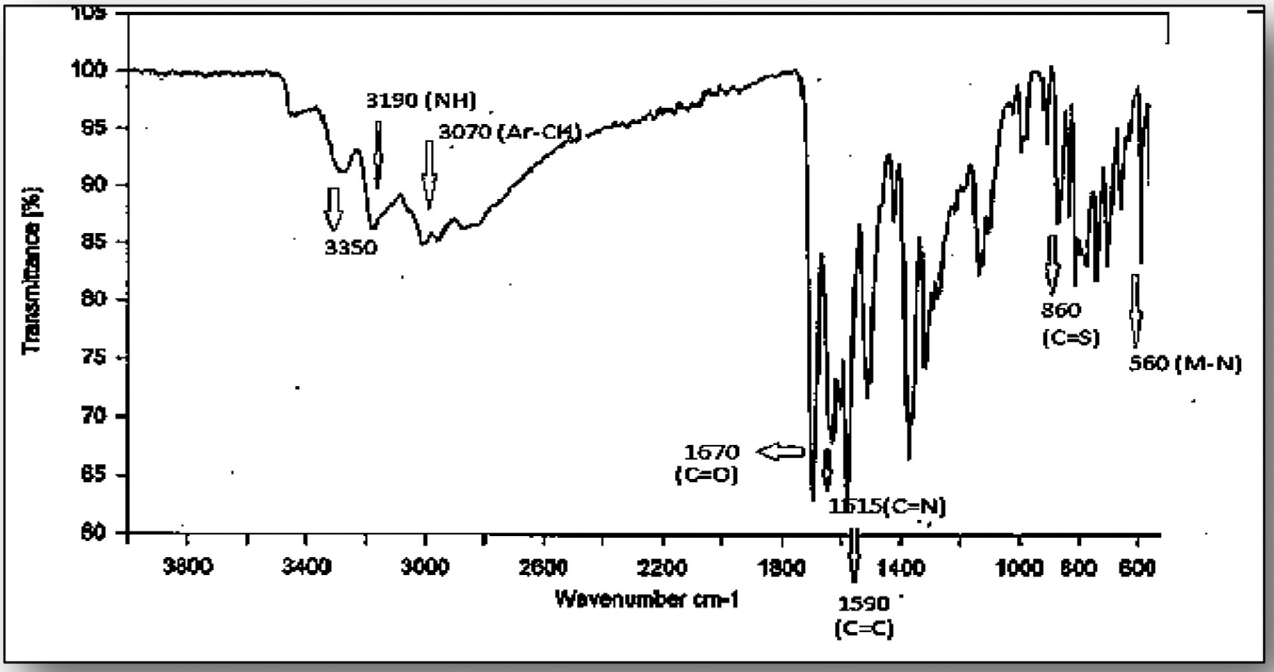

Fig. 4. IR spectrum of complex **5a**.

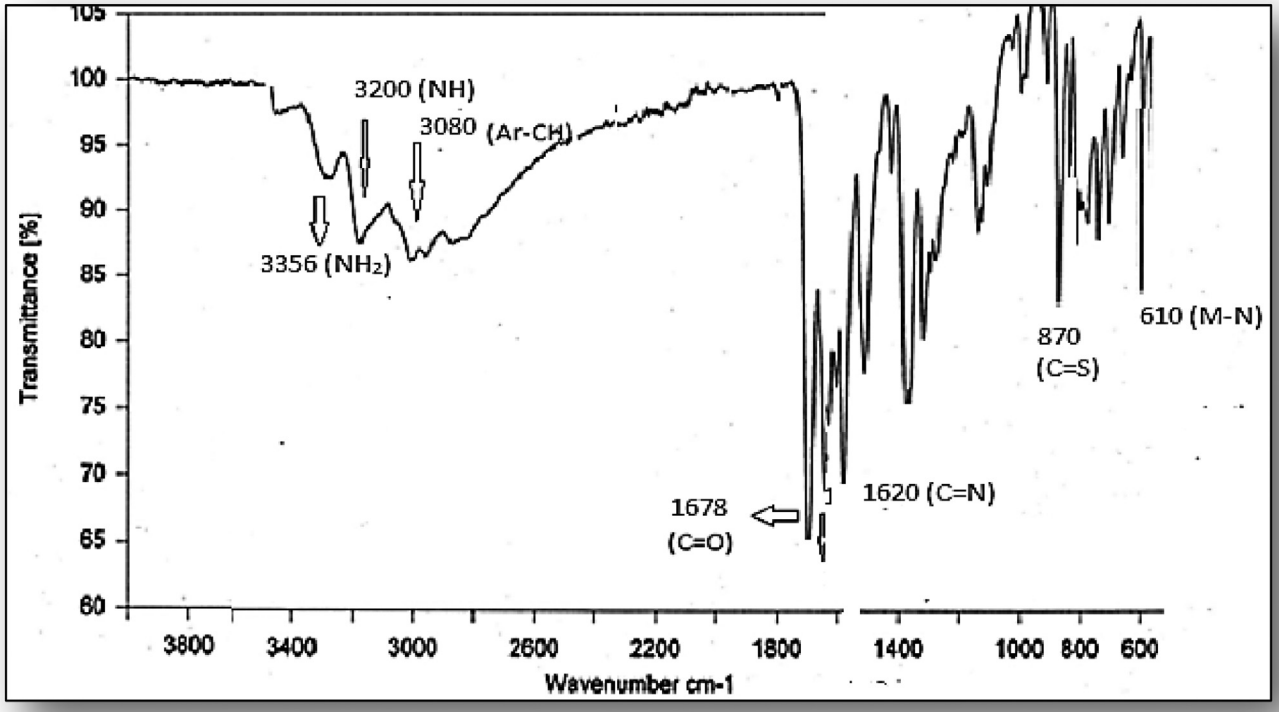

Fig. 5. IR spectrum of complex **7a**.

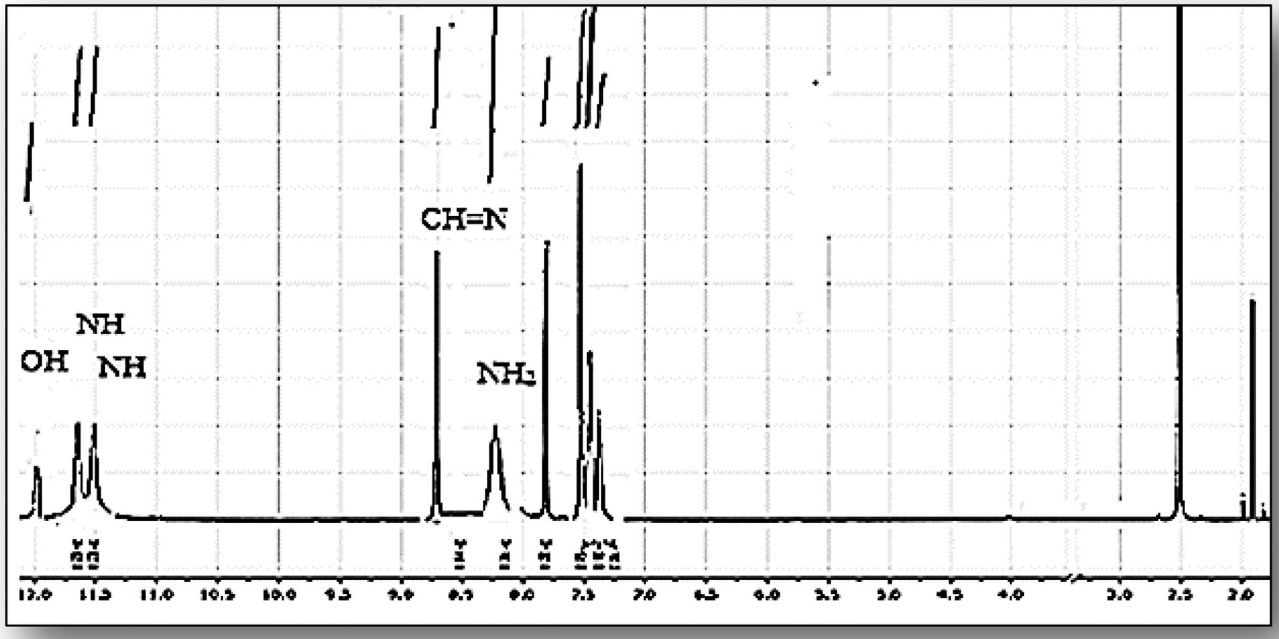

Fig. 6. ^{1}H NMR spectrum of Cu(I) metal complex **5a** formed between **3a** and Cu(I)I.

Table 3
IR absorption bands (ν, cm^{-1}) of ligands and their Cu(I), Cu(II) and Ni(II) complexes

Ligand	Absorption of functional groups (ν) in ligands (cm^{-1})	Metal Complex	Absorption of functional groups (ν) in complexes (cm^{-1})
3a	$\nu(NH_2)$: 3340, ν(w, strerch, NH): 3180, ν(strerch, Ar-CH): 3060, ν(s, stretch, C=O): 1665, ν(s, stretch, C=N): 1608, ν (bending, C=S): 850.	**5a**	$\nu(NH_2)$: 3350, ν(w, strerch NH): 3190, ν(Ar-CH): 3070, ν(C=O): 1670, ν(s, stretch, C=N): 1615, ν (C=S): 860 s, ν (M-N): 560 s.
3b	ν(OH): 3410 $\nu(NH_2)$: 3310, (w, strerch, NH): 3210, ν(strerch, Ar-CH): 3010, ν(s, stretch, C=O): 1665, ν(s, stretch, C=N): 1612, ν(bending, C=S): 820.	**5b**	ν(OH): 3425, $\nu(NH_2)$: 3325, (w, strerch, NH): 3220, ν(strerch, Ar-CH): 3015, ν(s, stretch, C=O): 1670, ν(s, stretch, C=N): 1620, ν (C=S): 827, ν(M-N): 585
3c	ν(OH): 3430, $\nu(NH_2)$: 3320, ν (w, strerch, NH): 3210, ν(strerch, Ar-CH): 3150, ν(s, stretch, C=O): 1680, ν(s, stretch, C=N): 1620, ν(bending, C=S): 840 s.	**5c**	ν(OH): 3450, $\nu(NH_2)$: 3330, ν(w, strerch, NH): 3220, ν(Ar-CH): 3170, ν(s, stretch, C=O): 1686, ν(s, stretch, C=N): 1630, ν (C=S): 850 s, ν(M-N): 592
3a	As before.	**7a**	$\nu(NH_2)$: 3356, ν(w, strerch NH): 3200, ν(Ar-CH): 3080, ν(s, stretch, C=O): 1678, ν(s, stretch, C=N): 1620, ν (bending, C=S): 870 s, ν (M-N): 610s.
3b	As before	**7b**	ν(OH): 3475, $\nu(NH_2)$: 3350 (w, strerch, NH): 3230, ν(Ar-CH): 3015, ν(s, stretch, C=O): 1680, ν(s, stretch, C=N): 1650, ν (bending, C=S): 850, ν(M-N): 610
3c	As before	**7c**	ν(OH): 3470, $\nu(NH_2)$: 3340, ν(w, strerch, NH): 3235, ν(Ar-CH): 3180, ν(C=O): 1692, ν(s, stretch, C=N): 1635, ν (bending, C=S): 880 s, ν(M-N): 620
3d	ν(w, strerch, OH): 3380, $\nu(NH_2)$: 3280, (w, strerch, NH): 3180, ν(Ar-CH): 3060, ν(s, stretch,C=O): 1656, ν(C=N): 1608, ν (bending, C=S): 815 s.	**7d**	ν(OH): 3398, $\nu(NH_2)$: 3290,(w, strerch, NH): 3195, ν(s, stretch, C=O): 1665, ν(s, stretch, C=N): 1620, ν(bending, C=S): 825 s, ν(M-N): 626 (M-N).
3e	ν(w, strerch, OH): 3385, $\nu(NH_2)$: 3250, (w, strerch, NH): 3208, ν(strerch, Ar-CH): 3071, ν(s, stretch, C=O): 1660, ν(s, stretch, C=N): 1622, ν (bending, C=S): 830 s.	**7e**	ν(OH): 3392, $\nu(NH_2)$: 3260, (w, strerch, NH): 3212, ν(s, stretch, C=O): 1680, ν(s, stretch, C=N): 1630, ν(bending, C=S): 850, ν(M-N): 620 (M-N).
3f	ν(OH): 3390, $\nu(NH_2)$: 3100, (w, strerch, NH): 3040, ν(strerch, Ar-CH): 3060, ν(s, stretch, C=O): 1665, ν(s, stretch, C=N): 1616, ν(C=S): 825 s.	**7f**	ν(OH): 3400, $\nu(NH_2)$: 3260, (w, strerch, NH): 3160, ν(s, stretch, C=O): 1672, ν(s, stretch, C=N): 1635, ν(bending, C=S): 835, ν(M-N): 620
3g	ν(OH): 3370, $\nu(NH_2)$: 3260, (w, strerch, NH): 3010, ν(strerch, Ar-CH): 3070, ν(s, stretch, C=O): 1665, ν(s, stretch, C=N): 1618, ν(bending, C=S): 820 s.	**7g**	ν(OH): 3400, $\nu(NH_2)$: 3280,(w, strerch NH): 3150, ν(s, stretch, C=O): 1675, ν(s, stretch, C=N): 1630, ν(bending, C=S): 830, ν(M-N): 640.
3h	ν(OH): 3367, $\nu(NH_2)$: 3240, (w, strerch, NH): 3150, ν(strerch, Ar-CH): 3060, ν(s, stretch, C=O): 1660, ν(s, stretch, C=N): 1620, ν(bending, C=S): 820 s.	**7h**	ν(OH): 3420, $\nu(NH_2)$: 3280, (w, strerch, NH): 3180, ν(s, stretch, C=O): 1670, ν(s, stretch, C=N): 1630, ν (bending, C=S): 830, ν(M-N): 615

Table 4
Chemical shifts (d) including 1H and 13C NMR spectroscopic data for ligands **3a,b** and Cu(I)-complexes of 5a-c.

No	Compound	^{1}H and ^{13}C NMR (δ, DMSO-d_6)
1	**3a**	δ_H 7.23-7.27 (m, 1H, ArH), 7.47-7.51 (m, 2H, Ar-H), 8.14 (bs, 2H, NH_2), 8.53 (bs, 1H, HC=N), 11.53 (bs, 1H, NH), 11.64 (bs, 1H, NH), 11.69 (bs, 1H, OH); δ_C 103.2 (C-3), 110.2, 115.0, 117.5 (Ar-CH), 123.7, 126.0 (C-6), 134.1, 136.1 (Ar-C), 145.7 (HC=N), 161.6 (C=O), 168.2 (C-4), 176.3 (C=S).
2	**5a**	δ_H 7.30-7.37 (m, 1H, ArH), 7.50-7.62 (m, 2H, Ar-H), 8.30 (bs, 2H, NH_2), 8.60 (bs, 1H, HC=N), 11.65 (bs, 1H, NH), 11.90 (bs, 1H, NH), 11.80 (bs, 1H, OH); δ_C 106.0 (C-3), 112.0, 116.0, 120.0 (Ar-CH), 124.0, 128.0 (C-6), 135.0, 136.0 (Ar-C), 146.80 (HC=N), 163.0 (C=O), 169.0 (C-4), 180.0 (C=S).
3	**3b**	δ_H 7.36-7.38 (dd, J = 7.38, 4.6 Hz, 1H, Ar-H), 7.44-7.46 (d, 1H, J = 8.6 Hz, Ar-H), 7.80-7.83 (d, 1H, J = 8.6 Hz, Ar-H), 8.14 (bs, 2H, NH_2), 8.52 (bs, 1H, HC=N), 11.51 (bs, 1H, NH), 11.52 (bs, 1H, NH), 11.65 (bs, 1H, OH); δ_C 103.27 (C3), 116.25 (C5), 118.73, 125.95, 129.49 (CH-Ar), 132.99, 140.26 (Ar-C), 145.88 (HC=N), 161.42 (C=O), 162.06 (C4), 172.49 (C=S).
4	**5b**	δ_H 7.40-7.42 (dd, J = 7.3, 4.2 Hz, 1H, Ar-H), 7.50-7.53 (d, 1H, J = 8.6 Hz, Ar-H), 7.90-7.93 (d, 1H, J = 8.6 Hz, Ar-H), 8.50 (bs, 2H, NH_2), 8.60 (bs, 1H, HC=N), 11.65 (bs, 1H, NH), 11.70 (bs, 1H, NH), 11.95 (bs, 1H, OH); δ_C 104.2 (C-3), 117.0 (C-5), 118.7, 126.0, 129.4 (CH-Ar), 133.9, 140.0 (Ar-C), 148.0 (HC=N), 163.0 (C=O), 164.0 (C-4), 175.5 (C=S).
6	**5c**	δ_H 7.40-7.60 (m, 3H, ArH), 8.30 (bs, 2H, NH_2), 8.60 (bs, 1H, HC=N), 11.60 (bs, 1H, NH), 11.84 (bs, 1H, NH), 12.20 (bs, 1H, OH); δ_C 105.0 (C-3), 110.0, 117.4, 118.0 (Ar-CH), 122.8, 126.9 (C-6), 133.4, 136.2 (Ar-C), 147.0 (HC=N), 163.4 (C=O), 168.6 (C-4), 177.2 (C=S).

metal complex and the RNA dependent RNA polymerase (RdRp) complex and also gave us a fair conclusive idea of their potential to act as an inhibitor in preventing the RNA replication process in the cells infected by SARS-CoV-2 and creating new virions. In addition to evaluate the effect of metal complexation with the ligands in binding to the active site in comparative to the ligands itself, the docking scores of the tested compounds are depicted in Table 5 that used to calculate the inhibition constant (*Ki* value) according to the reported equation [33] (see supplementary data).

Typically, a high potency is implied by a low *Ki* value and it should be in the micromolar range for a molecule to be qualified as a hit or lead compound. Compounds **7d** and **7e** have the least

Table 5
Energy scores for the complexes formed by the optimized structures of tested complexes 5a,b and 7a-f and their corresponding ligands 3a-f in the active site of the RdRp complex of SARS-CoV-2. (PDB ID: 6M71).

Compound	S Score	C-Docker energy (Kcal/mole)	inhibition constant (ki = μM)	Ligand-Receptor Interaction Residue	Type	Length (Å)
5a	-6.56	-3.9	1.57×10^{-5}	ASP623	H-donor	3.43
		20.1		ARG553	H-acceptor	3.02
		2.27		ASP623	metal	2.27
5b	-6.45	-4.3	1.89×10^{-5}	ASP623	H-donor	3.37
		17.0		ARG553	H-acceptor	3.03
		-3.6		ASP623	metal	2.22
7a	-7.98	-5.9	1.43×10^{-6}	ASP623	H-donor	2.93
		-2.7		THR556	H-acceptor	3.33
		17.1		ARG553	H-acceptor	2.94
		7.4		ARG553	H-acceptor	3.18
		-0.8		ASP623	Metal	2.43
		-0.6		LYS621	Pi-cation	3.87
7b	-8.05	-2.2	1.3×10^{-6}	ASP618	H-donor	3.49
		-0.7		ASP623	H-donor	3.37
		-2.6		ASP623	H-donor	2.73
		-1.5		ASP623	H-donor	3.19
		7.0		ARG553	H-acceptor	2.89
		4.1		THR556	H-acceptor	3.21
		-1.9		ASP623	Metal	2.35
		-1.0		LYS621	Pi-H	4.29
		-0.6		LYS621	Pi-cation	4.46
7c	-8.31	-3.3	8.25×10^{-7}	TYR619	H-donor	3.22
		-5.6		TYR619	H-acceptor	3.50
		13.5		ARG553	H-acceptor	2.88
		-0.6		LYS621	Pi-H	3.99
7d	-9.69	-0.6	8.06×10^{-8}	ASP623	H-donor	3.09
		3.04		ARG553	H-acceptor	3.04
7e	-8.99	-1.8	2.6×10^{-7}	ASP623	H-donor	3.30
		-10.7		ASP623	H-donor	3.10
		-4.1		ASP623	H-donor	3.12
		43.6		ARG553	H-acceptor	3.02
		-6.7		ARG553	H-acceptor	3.24
		19.0		THR556	H-acceptor	2.98
		-1.3		LYS621	Pi-cation	3.75
7f	-8.74	-3.9	3.49×10^{-7}	ASP623	H-donor	3.11
		-9.6		ASP623	H-donor	3.17
		-1.8		ASP623	H-donor	3.18
		48.1		ARG553	H-acceptor	2.98
		-5.3		THR556	H-acceptor	3.40
		20.9		ARG553	H-acceptor	2.87
		-1.3		LYS621	Pi-cation	3.80
3a	-5.35	-3.6	1.21×10^{-4}	ASP623	H-donor	2.82
		-2.3		ARG553	H-acceptor	4.04
		-5.7		ARG553	H-acceptor	3.54
		-4.7		ARG555	H-acceptor	3.95
		-3.7		ARG555	H-acceptor	3.99
3b	-5.48	-4.6	9.73×10^{-5}	ASP623	H-donor	2.80
		-2.3		ARG553	H-acceptor	4.02
		-5.7		ARG553	H-acceptor	3.51
		-4.8		ARG555	H-acceptor	3.93
		-3.7		ARG555	H-acceptor	3.96
		-0.7		LYS621	Pi-cation	3.86
3c	-5.89	-1.7	4.88×10^{-5}	THR556	H-donor	2.84
		-3.1		SER682	H-acceptor	3.73
3d	-5.39	-3.6	1.13×10^{-4}	ASP623	H-donor	2.81
		-2.3		ARG553	H-acceptor	4.03
		-5.7		ARG553	H-acceptor	3.54
		-4.7		ARG555	H-acceptor	3.96
		-3.6		ARG555	H-acceptor	4.01
		-0.6		ARG556	H-acceptor	4.04
3e	-5.45	-4.6	1.02×10^{-4}	ASP623	H-donor	2.78
		-2.4		ARG553	H-acceptor	3.97
		-5.7		ARG553	H-acceptor	3.50
		-4.9		ARG555	H-acceptor	3.96
		-3.4		ARG555	H-acceptor	4.04
		-0.7		ARG556	H-acceptor	4.38
		-0.8		LYS621	Pi-cation	3.89
3f	-5.19	-3.0	1.59×10^{-4}	ASP623	H-donor	2.85
		-2.7		ARG553	H-acceptor	4.07
		-4.9		ARG553	H-acceptor	3.65
		-4.6		ARG555	H-acceptor	3.93
		-2.4		ARG555	H-acceptor	4.06
		-1.1		ARG556	H-acceptor	4.24

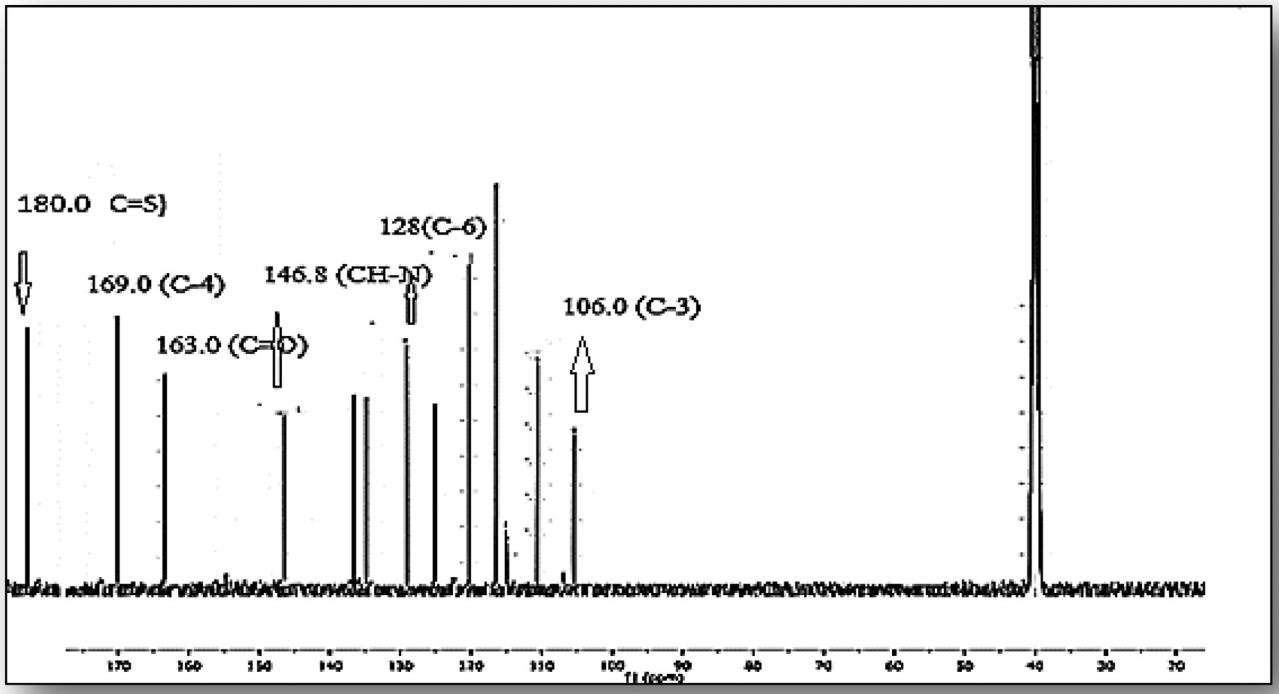

Fig. 7. ^{13}C NMR spectrum of Cu(I) metal complex **5a** formed between **3a** and Cu(I)I.

Table 6
Physicochemical and lipophilicity of the target compounds using Swiss ADME & Molinspiration software.

	Physicochemical properties									
Compound	Lipophilicity Consensus log P	MW[a] g/mol	Heavy atoms	Aromatic heavy atoms	Rot.bond	H-bond acc.	H-bond don.	MR[b]	TPSA[c](A^2)	% ABS[d]
5a	0.04	360.28	20	10	0	2	4	85.60	135.59	62.43
5b	0.11	404.73	20	10	0	3	5	88.29	135.59	62.43
7a	-0.68	698.07	42	20	3	4	6	160.60	249.46	22.94
7b	-0.11	799.75	40	20	1	4	8	176..58	271.18	15.56
7c	-1.20	641.96	38	20	1	4	8	161.18	271.18	15.56
7d	-1.23	655.99	39	20	1	4	7	166.08	260.32	19.19
7e	-0.22	720.56	40	20	1	4	8	171.20	271.18	15.56
7f	-0.10	809.46	40	20	1	4	8	176.58	271.18	15.56
7g	-0.22	720.56	40	20	1	4	8	171.20	271.18	15.56
7h	-0.10	809.46	40	20	1	4	8	176.58	271.18	15.56

Abbreviation: MW[a], molecular weight; MR[b], molar refractivity; TPSA[c], topological polar surface area; %ABS [d]: percentage of absorption.

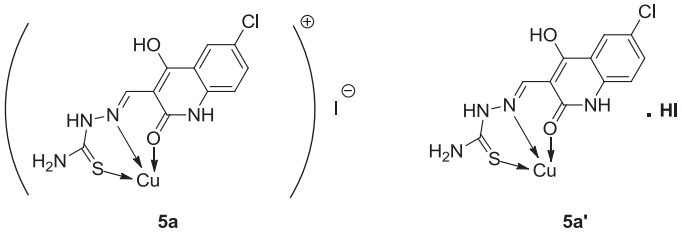

5a 5a'

Fig. 8. Structure of acidic form of compound **5a** as in **5a'**.

Ki value of 8.06 × 10^{-8} and 2.6 × 10^{-7} µM, respectively to qualify as a drug and hence, the most potent among the other tested compounds.

Prior to the molecular docking studies, the receptor protein was prepared for docking by deleting additional water and co-factors, followed by the addition of polar hydrogens and computing charges fixation.

Table 5 illustrates the binding free energies from the best favorable poses of the target complexes **5a,b** and **7a-f**. Most of the tested compounds have high binding affinity to the RdRp as the binding free energy (ΔG) values of them range from -10.7 to 43.6 Kcal/ mole better than their corresponding ligands **3a-f** (ΔG = -5.7 to -0.6 Kcal/mole). The docking study results of target complexes **5a,b** and **7a-f** showed better mode of interactions than their corresponding ligands **3a-f**, however, complexes of Cu(II) and Ni(II) exhibited better *S*-score than those of Cu(I).The 2D & 3D diagrams of the compounds showed crucial binding with ASP623 and ARG553 through quinoline and Cu(I)/ (II) or Ni functionality. Furthermore, stabilization of the complexes within the active site occurred through two strong hydrogen bond interactions with amino acid residue THR556 and LYS621. Compounds **7a**, **7b** and **7e** exhibited potential interactions with all the previous mentioned amino

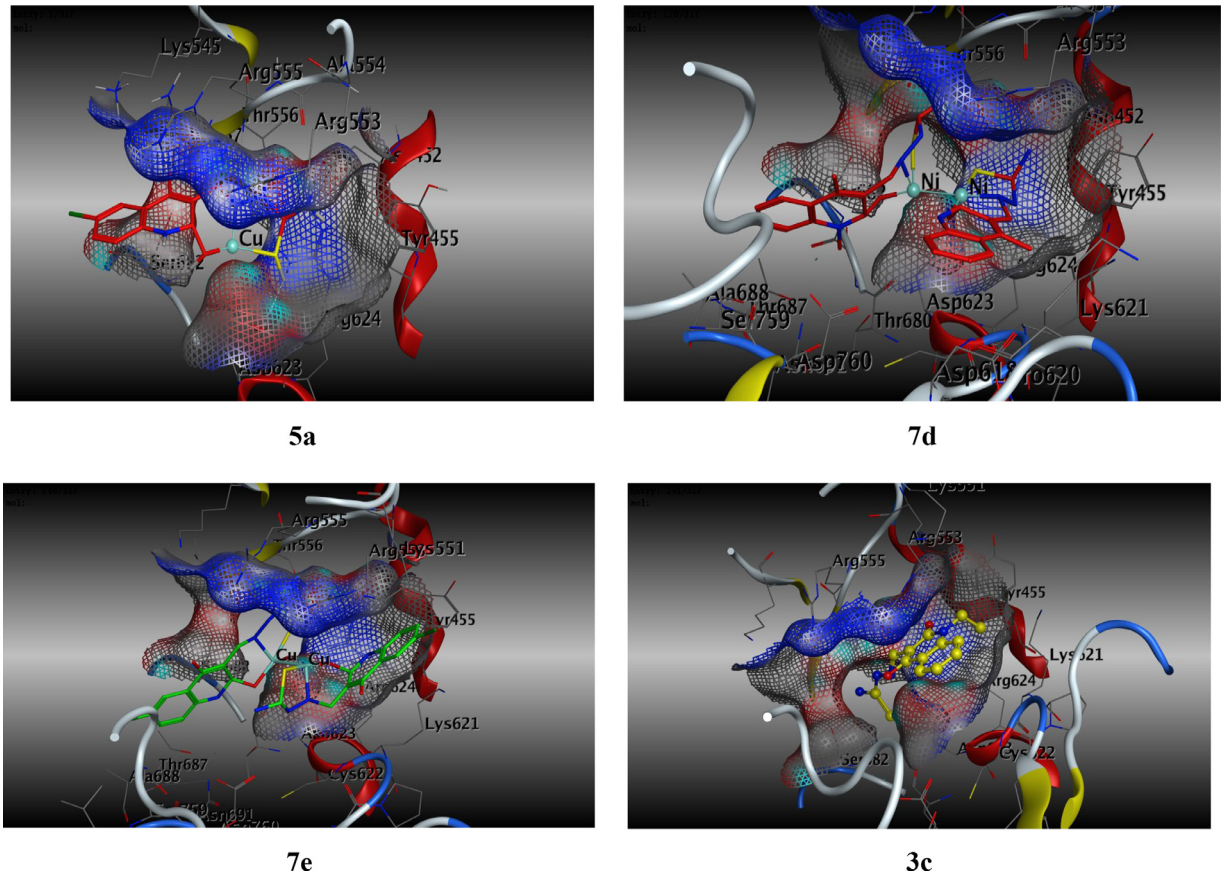

Fig. 9. 3D diagram of the molecular surface illustrating the binding modes of Cu(I)complex (**5a**), Ni(II) complex (**7d**), Cu(II) complex (**7e**) and the ligand (**3c**) (interacted with the active site of RdRp complex of SARS-CoV-2. (PDB ID: 6M71).

acid, however, all of the tested derivatives **5a,b** and **7a-f** possess interaction with ARG553 amino acid residue(See Fig. 9 for **7e**).

Most of the tested complexes showed interaction greater than their corresponding ligands to interact with the same amino acids with additional hydrogen bond interaction with THR556 which is lacked in ligands. On the other hand, Cu(I) complexes **5a** and **5b** dismissed hydrogen binding interactions with the amino acid residue THR556 and LYS137(See Fig.9 for **5a**) . Also, compound **7c** kept two hydrogen bond interactions with ARG553 and LYS621. The corresponding ligands **3a**, **3b** and **3d-f** showed additional H-bonding with ARG555 amino acid residue which is not observed with the complexes.

3.4.2. Prediction of physicochemical properties, pharmacokinetics, and drug-likeness profile in silico

Because of unacceptable ADME parameters (distribution, excretion, absorption and metabolism), in addition to the costs needed for developing a new drug. Design and applied new drugs is considered to be complicated. Hence, estimating the pharmacokinetic properties of a new drug is a critical step in the process of drug development and can directly contribute to optimization efforts into recovered analogs [34]. Recently, The most promising compounds can be picked *in silico* ADMET screens, reducing the chance of degradation of drugs in late stages [35]. To achieve a desired *in vivo* goal, it should be balance between pharmacodynamics and pharmacokinetic properties. Also, Further information about regimen and drug dose are given by the prediction of brain penetration, volume of distribution, oral bioavailability, and clearance [36]. Many parameters such as drug solubility S, partition coefficients, polar surface PSA, cell permeability, human intestinal absorption HIA, and drug-likeness score have been studied during virtual screening

Table 7
Lipinski drug-likeness of the target compounds using Molsoft & SwissADME software.

Code	S[a] (mg/L)	Drug likeness model score	Lipinski violations	Bioavailability score
5a	1.90	-0.43	0	0.55
5b	2.69	-0.03	0	0.55
7a	1.39	0.41	3	0.17
7b	3.88	-0.59	3	0.17
7c	9.09	0.38	3	0.17
7d	2.67	0.38	3	0.17
7e	7.22	-0.03	3	0.17
7f	3.78	-0.43	3	0.17
7g	7.22	-0.03	3	0.17
7h	3.78	-0.43	3	0.17

[a] S: solubility

methods. An available orally drug elected in agreement with Lipinski's rule If the molecular weight is less than 500, Log P is not higher than 5, the number of hydrogen bond acceptors is less than 10 and the number of donor hydrogen bond donors is less than 5 [37]. The number of rotatable bonds reflects molecular flexibility that plays an important role in oral bioavailability and means less orally active in a flexible molecule. The number of hydrogen bonding groups has also been suggested as a consideration to substitute for the polar surface area (PSA) and also to measure the percentage absorption (%ABS) as it is in inversely proportional to tPSA

$$\%ABS = 109 - 0.345\ tPSA.$$

The higher oral bioavailability exhibited by Compounds with tPSA of less than 140 A^2 and 10 or fewer rotatable bonds [34].

Table 8
ADME data of tested compounds calculated using preADMET software.

code	Pharmacokinetics								
	GI absorption[a]	BBB permeant[b]	P-gp substrate[c]	CYP1A2 inhibitor[d]	CYP2C19 inhibitor[e]	CYP2C9 inhibitor[f]	CYP2D6 inhibitor[g]	CYP3A4 inhibitor[h]	Log Kp (skin permeation
5a	High	High	High	Yes	no	no	no	no	-7.00
5b	High	High	Yes	Yes	Yes	yes	no	no	-7.49
7a	Low	No	Yes	No	no	no	no	no	-7.73
7b	Low	No	Yes	No	no	no	no	no	-8.09
7c	Low	No	Yes	No	no	no	no	no	-8.11
7d	Low	No	Yes	No	no	no	no	no	-8.10
7e	Low	No	Yes	No	no	no	no	no	-7.70
7f	Low	No	Yes	No	no	no	no	no	-8.10
7g	Low	No	Yes	No	no	no	no	no	-8.15
7h	Low	No	Yes	No	no	no	no	no	-8.15

[a]GI absorptiona: gastrointestinal absorption; [b]BBBb: blood-brain barrier penetration; [c]P-gp substratec: P-glycoprotein substrate; [d]CYP1A2 inhibitord: cytochrome P450 1A2 inhibitor; [e]CYP2C19 inhibitore: cytochrome P450 2C19 inhibitor; [f]CYP2C9 inhibitorf: cytochrome P450 2C9 inhibitor; [g]CYP2D6 inhibitorg: cytochrome P450 2D6 inhibitor; [h]CYP3A4 inhibitorh: cytochrome P450 3A4 inhibitor

Herein, we used Molinspiration [36], Molsoft [37], and SwissADME software [35] for predicting the pharmacokinetic parameters of the reported compounds. The results are shown in Table 7 exhibit that compounds **5a** and **5b** obey the Lipinski's rule with Log P values 0.04 and 0.11 (<5), respectively, an MW 360.28 and 404.73 (<500), HBD from 4 to 5 (≤ 5) and HBA from 2 to 3 (<10) (Table 6). They would theoretically show a strong oral absorption and this property cannot be attributed to variations in their bioactivity. Besides, the topological PSA values of the compounds ring of 135.69 (< 140A2) and the corresponding percentage oral absorption was between 15.6 and 62.4%, exhibit strong permeability, absorption and transport across biological membrane. Furthermore, the drug-likeness model score and solubility for compounds was confirmed by Molsoft software (Table 7) Aqueous solubility can change the absorption and distribution characteristics. the more positive drug-likeness model scores, the more likely it is to be drug molecule, these compounds have fulfilled their solution ability specifications at values between 1.39 and 9.09 mg / l (above 0.0001 mg /L). A positive model-scores (0.07 and 0.29, respectively) were anticipated for compounds **7a** and **7d** while that for other compounds was negative (-0.03 to -0.59).

Additionally, the following pharmacokinetic parameters were experimented *in silico* using SwissADME software: GI absorption, P-gp substrate, CYP1A2 inhibitor, CYP2C19 inhibitor, CYP2C9 inhibitor, CYP2D6 inhibitor and CYP3A4 inhibitor. The results of the ADME parameters are shown in (Table 8). The findings from compounds with low CNS absorption for most of the complexes; investigated compounds exhibited medium to low skin permeability Log K*p* range from -7.00 to -8.15. This is aligned with non-inhibitors of the CYP2D6 enzyme and thus may pretend no interactions with CYP2D6 inhibitors and/or inducers. Furthermore, they showed high human intestinal absorption for complexes **5a** and **5b** indicating very well-absorbed compounds. The examined compounds were found to be highly-bound to human glycoproteins.

4. Conclusion

The work in this paper describes the formation of new monodentate and bidentate metal complexes of thiosemicarbazones derived by 2-quinolones. FT-IR, ^{1}H NMR and mass spectroscopy together with elemental analysis confirmed the structure of the formed complexes. Furthermore, the molecular docking study was performed on the active site of RdRp complex of SARS-CoV-2 revealing a good interaction with the enzyme whereas Ni(II) and Cu(II) quinoline based complexes, showed better binding affinity of remarkable inhibition constant *Ki* in micromolar scale than their corresponding ligands. Additionally, preliminary *in silico* ADMET prediction indicated that these compounds could be good safe as candidates against COVID-19 that might be better alternatives of the current drugs to prevent SARS-CoV-2 and warrant further *in vitro/in vivo* application.

Declaration of Competing Interest

I would like to confirm that the my MS entitled Metal complexes of thiosemicarbazones derived by 2-quinolones with Cu(I), Cu(II) and Ni(II); identification by NMR, IR, ESI mass spectra and *in silico* approach as potential tools against SARS-CoV-2 has no declaration of interest.

Acknowledgements

Authors thank the CRC 3MET (TR88) for the support for one month to Professor Aly in September 2017.

Supplementary materials

Supplementary material associated with this article can be found, in the online version, at doi:10.1016/j.molstruc.2022.133480.

References

[1] D.C. Reis, A.A.R. Despaigne, J.G. Da Silva, N.F. Silva, C.F. Vilela, I.C. Mendes, J.A. Takahashi, H. Beraldo, Structural studies and investigation on the activity of imidazole-derived thiosemicarbazones and hydrazones against crop-related fungi, Molecules 18 (2013) 12645–12662.
[2] H. Beraldo, D. Gambino, Mini-Rev. The wide pharmacological versatility of semicarbazones, thiosemicarbazones and their metal complexes, Med. Chem 4 (2004) 31–39.
[3] D.C. Quenelle, K.A. Keith, E.R. Kern, *In vitro* and *in vivo* evaluation of isatin-beta-thiosemicarbazone and marboran against vaccinia and cowpox virus infections, Antivir. Res. 71 (2006) 24–30.
[4] A. Molter, J. Rust, C.W. Lehmann, G. Deepa, P. Chiba, F. Mohr, Synthesis, structures and anti-malaria activity of some gold(I) phosphine complexes containing seleno- and thiosemicarbazonato ligands, Dalton Trans. 40 (2011) 9810–9820.
[5] S. Arora, S. Agarwal, S. Singhal, Anticancer activities of thiosemi-carbazides/thiosemicarbazones: a review, Int. J. Pharm. Pharm. Sci. 6 (9) (2014) 34–41.
[6] Y. Yu, D.S. Kalinowski, Z. Kovacevic, A.R. Siafakas, P.J. Jansson, C. Stefani, D.B. Lovejoy, P.C. Sharpe, P.V. Bernhardt, D.R. Richardson, Thiosemicarbazones from the old to new: iron chelators that are more than just ribonucleotide reductase inhibitors, J. Med. Chem. 52 (2009) 5271–5294.
[7] H. Steinhagen, The evolution of drug discovery: from traditional medicines to modern drugs. By Enrique Raviña, ChemMedChem 6 (2011) 1746–1747.
[8] R.W. Brockman, J.R. Thomson, M.J. Bell, H.E. Skipper, Observations on the antileukemic activity of pyridine-2-carboxaldehyde thiosemicarbazone and thiocarbohydrazone, Cancer Res. 16 (1956) 167–170.
[9] R.A. Finch, M.C. Liu, A.H. Cory, J.G. Cory, A.C. Sartorelli, Triapine (3-aminopyridine-2-carboxaldehyde thiosemicarbazone; 3-AP): an inhibitor of ribonucleotide reductase with antineoplastic activity, Adv. Enzyme Regul. 39 (1999) 3–12.

[10] A.M. Traynor, J.-W. Lee, G.K. Bayer, J.M. Tate, S.P. Thomas, M. Mazurczak, D.L. Graham, J.M. Kolesar, J.H. Schiller, A phase II trial of Triapine® (NSC# 663249) and gemcitabine as second line treatment of advanced non-small cell lung cancer: eastern cooperative oncology group study 1503, Invest. New Drugs 28 (2010) 91–97.
[11] S. Wadler, D. Makower, C. Clairmont, P. Lambert, K. Fehn, M. Sznol, Phase I and pharmacokinetic study of the ribonucleotide reductase inhibitor, 3-aminopyridine-2- carboxaldehyde thiosemicarbazone, administered by 96-hour intravenous continuous infusion, J. Clin. Oncol. 22 (2004) 1553–1563.
[12] M.J. Mackenzie, D. Saltman, H. Hirte, J. Low, C. Johnson, G. Pond, M.J. Moore, A Phase II study of 3-aminopyridine-2-carboxaldehyde thiosemicarbazone (3-AP) and gemcitabine in advanced pancreatic carcinoma. A trial of the princess Margaret hospital phase II consortium invest, New Drugs 25 (2007) 553–558.
[13] J. Kolesar, R.C. Brundage, M. Pomplun, D. Alberti, K. Holen, A. Traynor, P. Ivy, G. Wilding, Population pharmacokinetics of 3-aminopyridine-2-carboxaldehyde thiosemicarbazone (Triapine®) in cancer patients, Cancer Chemother. Pharmacol 67 (2011) 393–400.
[14] J.E. Karp, F.J. Giles, I. Gojo, L. Morris, J. Greer, B. Johnson, M. Thein, M. Sznol, J. Low, A phase I study of the novel ribonucleotide reductase inhibitor 3-aminopyridine-2-carboxaldehyde thiosemicarbazone (3-AP, Triapine®) in combination with the nucleoside analog fludarabine for patients with refractory acute leukemias and aggressivemyeloproliferative disorders, Leuk. Res. 32 (2008) 71–77.
[15] J.F. Zeidner, J.E. Karp, A.L. Blackford, B.D. Smith, I. Gojo, S.D. Gore, M.J. Levis, H.E. Carraway, J.M. Greer, S.P. Ivy, K.W. Pratz, M.A. McDevitt, A phase II trial of sequential ribonucleotide reductase inhibition in aggressive myeloproliferative neoplasms, Haematologica 99 (2014) 672–678.
[16] J. Chen, Y. Huang, G. Liu, Z. Afrasiabi, E. Sinn, S. Padhye, Y. Ma, The cytotoxicity and mechanisms of 1,2-naphthoquinone thiosemicarbazone and its metal derivatives against MCF-7 human breast cancer cells, Toxicol. Appl. Pharmacol. 197 (2014) 40–48.
[17] B.M. Paterson, P.S. Donnelly, Copper complexes of bis(thiosemicarbazones): from chemotherapeutics to diagnostic and therapeutic radiopharmaceuticals, Chem. Soc. Rev. 40 (2011) 3005–3018.
[18] H. Huang, Q. Chen, X. Ku, L. Meng, L. Lin, X. Wang, C.X. Zhu, Y. Wang, Z. Chen, M. Li, H. Jiang, K. Chen, J. Ding, H. Liu, A series of α-heterocyclic carboxaldehyde thiosemicarbazones inhibit topoisomerase IIα catalytic activity, J. Med. Chem. 53 (2010) 3048–3064.
[19] B.M. Zeglis, V. Divilov, J.S. Lewis, Role of metalation in the topoisomerase IIα inhibition and antiproliferation activity of a series of α-heterocyclic-N^4-substituted thiosemicarbazones and their Cu(II) complexes, J. Med. Chem. 54 (2011) 2391–2398.
[20] B. Sever, H. Soybir, S. Görgülü, Z. Cantürk, M.D. Altıntop, Pyrazole incorporated new thiosemicarbazones: design, synthesis and investigation of DPP-4 inhibitory effect, Molecules 25 (2020) 1–19 5003.
[21] V.H. Pham, T.P.D. Phan, D.C. Phan, B.D. Vu, Synthesis and bioactivity of thiosemicarbazones containing adamantane skeletons, Molecules 25 (2020) 1–14 324.
[22] N.S. Youssef, A.M.A. El-Seidya, M. Schiavoni, B. Castano, F. Ragaini, E. Gallo, A. Caselli, Thiosemicarbazone copper complexes as competent catalysts for olefin cyclopropanations, J. Organomet. Chem. 714 (2012) 94–103.
[23] J.G. Da Silva, A.A. Recio Despaigne, S.R. Louro, C.C. Bandeira, E.M. Souza-Fagundes, H. Beraldo, Cytotoxic activity, albumin and DNA binding of new copper(II) complexes with chalcone-derived thiosemicarbazones, Eur. J. Med. Chem. 65 (2013) 415–426.
[24] S.I. Orysyk, G.G. Repich, V.V. Bon, V.V. Dyakonenko, V.V. Orysyk, Yu.L. Zborovskii, O.V. Shishkin, V.I. Pekhnyo, M.V. Vovk, Novel Fe(III), Co(III), Ni(II), Cu(II) coordination compounds involving 2-[(2-hydroxyphenyl)methylene]hydrazine-*N*-(2-propenyl)-carbothioamide as ligand: synthesis, crystal structures and spectral characteristics, Inorg. Chim. Acta 423 (2014) 496–503.
[25] P.F. Rapheal, E. Manoj, M.R.P. Kurup, H.K. Fun, Nickel(II) complexes of *N*(4)-substituted thiosemicarbazones derived from pyridine-2-carbaldehyde: crystal structures, spectral aspects and Hirshfeld surface analysis, J. Molecular Struct. 1237 (2021) 130362.
[26] A.A Cortes, J.M. Zuñiga, The use of copper to help prevent transmission of SARS-Corona virus and influenza viruses. A general review, Diagn. Microbiol. Infect. Dis. 98 (4) (2020) 115176.
[27] A.K. Moharana, R.N. Dash, B.B. Subudhi, Thiosemicarbazides: updates on antivirals strategy, Mini Rev. Med. Chem. 20 (2020) 2135–2152.
[28] L. de P. Fernandes, J.M.B. Silva, D.O.S. Martins, M.B. Santiago, C.H.G. Martins, A.C.G. Jardim, G.S. Oliveira, M.P.R.A.C. Souza, E. de F. Franca, V.M. Deflon, A.E.H. Machado, C.G. Oliveira, Fragmentation study, dual anti-bactericidal and anti-viral effects and molecular docking of cobalt(III) complexes, Int. J. Mol. Sci. 21 (2020) 8355.
[29] Y.Y. Gao, L. Yan, Y. Huang, F. Liu, Y. Zhao, L. Cao, T. Wang, Q. Sun, Z. Ming, L. Zhang, J. Ge, L. Zheng, Y. Zhang, H. Wang, Y. Zhu, C. Zhu, T. Hu, T. Hua, B. Zhang, X. Yang, J. Li, H. Yang, Z. Liu, W. Xu, L.W. Guddat, Q. Wang, Z. Lou, Z. Rao, Structure of the RNA-dependent RNA polymerase from COVID-19 virus, Science 368 (2020) 779–782.
[30] A. Daina, O. Michielin, V. Zoete, SwissADME: a free web tool to evaluate pharmacokinetics, drug-likeness and medicinal chemistry friendliness of small molecules, Sci. Rep. 7 (2017) 42717.
[31] A.A. Aly, A.H. Mohamed, M. Ramadan, Synthesis and colon anticancer activity of some novel thiazole/-2-quinolone derivatives, J. Mol. Struct. 1207 (2020) 127798.
[32] H. van de Waterbeemd, E. Gifford, ADMET *in silico* modelling: towards prediction paradise? Nat. Rev. Drug Discov. 2 (2003) 192–204.
[33] C.W. Murray, D.A. Erlanson, A.L. Hopkins, G.M. Keserü, P.D. Leeson, D.C. Rees, C.H. Reynolds, N.J. Richmond, Validity of ligand efficiency metrics, ACS Med. Chem. Lett. 5 (2014) 616–618.
[34] D.F. Veber, S.R. Johnson, H.Y. Cheng, B.R. Smith, K.W. Ward, K.D. Kopple, Molecular properties that influence the oral bioavailability of drug candidates, J. Med. Chem. 45 (2002) 2615–2623.
[35] E. Rajanarendar, S.R. Krishna, D. Nagaraju, K.G. Reddy, B. Kishore, Y. Reddy, Environmentally benign synthesis, molecular properties prediction and anti-inflammatory activity of novel isoxazolo[5,4-*d*]isoxazol-3-yl-aryl-methanones *via* vinylogous Henry nitroaldol adducts as synthons, Bioorg. Med. Chem. Lett. 25 (2015) 1630–1634.
[36] S. Wetzel, A. Schuffenhauer, S. Roggo, P. Ertl, H. Waldmann, Cheminformatic analysis of natural products and their chemical space, CHIMIA Int. J. Chem. 61 (2007) 355–360.
[37] Y.A. Arnautova, R.A. Abagyan, M. Totrov, Development of a new physics-based internal coordinate mechanics force field and its application to protein loop modeling, Proteins Struct. Funct. Bioinform. 79 (2011) 477–498.